A new rotary actuator capable of rapid motion using an antagonistic cam mechanism

AROB
Jimukyoku
Journal of Advances in Artificial Life Robotics, Vol. 1, No. 3 (December 2020) 143-151

A new rotary actuator capable of rapid motion using an antagonistic cam mechanism

Katsuaki Suzuki
Kyushu Institute of Technology, 2-4 Hibikino, Wakamatsu, Kitakyushu, Fukuoka 808-0196, Japan

Yuya Nishida
Kyushu Institute of Technology, 2-4 Hibikino, Wakamatsu, Kitakyushu, Fukuoka 808-0196, Japan

Takashi Sonoda
Nishinippon Institute of Technology, 1-11 Aratsu, Kanda, Miyako, Fukuoka 800-0394, Japan

Kazuo Ishii
Kyushu Institute of Technology, 2-4 Hibikino, Wakamatsu, Kitakyushu, Fukuoka 808-0196, Japan
E-mail: suzuki.katsuaki448@mail.kyutech.jp, ynishida@lsse.kyutech.ac.jp, ishii@brain.kyutech.ac.jp

Abstract

Animals can achieve agile behaviors such as jumping and throwing in addition to flexible behaviors with the same musculoskeletal systems, and those movements can extend the range of their activities. We have been working on actuators capable of rapid and flexible motions learning the musculoskeletal systems. In this paper, we propose a new rotary actuator using a pair of motors, springs, and cams to perform three functions, namely, normal motion, rapid or instantaneous motion, and rigidity control using an antagonistic cam mechanism, and describe the operating principle of the proposed mechanism, the mathematical model of the mechanism during rapid motion, and the design principle of the cam, which is a key mechanical element in this mechanism. Finally, we present an analysis of the error between the theoretical the measurement results during rapid motion.

Keywords: high-power joint, link mechanism, cam mechanism, design principle

1. Introduction

Robots are generally designed for necessary target tasks such as picking and walking with the negotiation of actuator power, structural strength, computer power, battery and so on. Designing a robot with additional functions such as jumping, throwing, and flexible contact movements causes the design conflict because of available actuators and materials, however, is one way of expanding the range of robot activity. Marc Raibert et al. developed one-, two-, and four-leg that can balance in the plane and in 3D in 1980s [1], [2] and currently the technologies are taken over to famous quadruped robots Big Dog and Spot. H. Okubo designed a jumper activated by small actuators using self-energizing springs [3]. S. Hyon and T. Mita developed robots able to jump, hop, and execute other gymnastic movements [4],[5],[6], and their robots realized biologically inspired hopping, multiple-DOF jumping, and multilink gymnastics. We have been working on actuators capable of rapid and flexible motions using energy charging system and proposed Inertia Actuator and Cam Charger [7], [8].

For jumping, it is necessary to accelerate the upper body first and then the entire body, including the actuator. The output part must be passively moved when an external force is applied to it to achieve flexible contact. It is difficult to realize these functions in a robot because a high-output general motor and reducer inevitably tend to be heavy. In addition, actuators that combine a motor and speed reducer generally do not exhibit back drivability. For robots to achieve rapid acrobatic movement and flexible contact movements, lightweight, high-power actuators and flexible actuators are necessary [9],[10],[11],[12]. The authors developed a high-power joint mechanism that mimics the rear leg of a locust. This mechanism is operated using a motor to realize an actuator with high stand-alone properties and various functions [13],[14]. The mechanism can realize normal motion and rapid motion and can control instantaneous force. When jumping, the locust stores energy in the elastic elements in the exoskeleton of its hind legs by simultaneously contracting the high-strength extensor muscles and the small flexor muscles [15],[16]. Then, by relaxing only the extensor muscle, it releases the stored power and jumps. During the contraction of the muscles, the flexor muscles use a portion called a ramp to increase the moment arm to compensate for the difference in force between the flexors and extensors. The mechanism developed by the authors comprises a link mechanism for the exoskeleton, a spring for the elastic element, a reducer with different reduction ratios, and a motor and wire for the extensor and flexor muscles to closely mimic the rear leg structure of the locust. The structure of the ramp is expressed by making the link ratio asymmetric. In rapid motion, the link corresponding to the leg is moved rapidly by removing the voltage applied to the motor on the flexor side after spring compression. However, at this time, the flexor side motor has a structure that rotates passively, and hence, the viscous resistance of the reducer affects it, and a large instantaneous force cannot be obtained. Furthermore, since the link ratio is asymmetric and the reduction ratios of the two motors are different, the rotation direction of the link corresponding to the leg is limited to one direction during the rapid motion.

In the present research, we proposed a new actuator locust-mimicking mechanism to realize functions such as normal motion, more powerful rapid motion, and the stiffness control of the main joint. The cam can set an arbitrary reduction ratio curve according to its shape. Since intermittent motion can be realized by abruptly changing the reduction ratio, the release mechanism with the cam realizes a release motion that is unaffected by viscosity [17],[18]. In addition, by adopting a symmetrical link ratio of the mechanism and using identical specifications for the two motors and reducers, it is possible to eliminate the restrictions on the rotation direction during rapid motion. In this paper, we describe the operating principle of the high-power joint mechanism with cams, the design principle of the cam, and the results of evaluation of the validity of applying an instantaneous force using an actual machine. The cams play an important role in this mechanism.

2. Overview of the proposed mechanism

The proposed mechanism is shown in Fig. 1. The mechanism consists of two motors, cams, cam followers, a passive link, wires, a slider, a linear shaft, a spring, a main joint, and an output link. The main feature of the proposed mechanism is that it has three functions: Normal motion, rapid motion, and rigidity control of the main joint. For normal motion, the output link moves with the same output (output = torque × speed) as the built-in motor. The output link is moved by rotating two cams that are coaxial with the motor in the same direction. In the case of rapid motion, the output link can move momentarily to generate more power than the built-in motor. When performing rapid motion, first the two cams are rotated in different directions to store energy in the spring. Next, the cam follower, which is in contact with the cam, moves away from the cam when it reaches the release-operation point. Thereafter, the stored energy is released. At this time, since the joint of the passive link is not affected by the viscous resistance of the motor reducer, the release operation is performed with minimal loss. After release, the slider performs translational motion using the force stored in the spring.

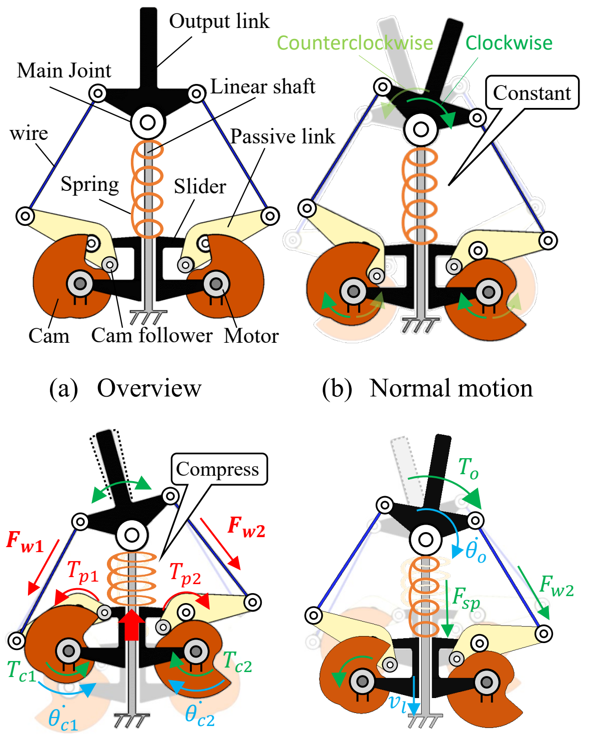

(a) Overview (b) Normal motion

(c) Charging (d) Rapid motion

Fig.1 Model of the proposed mechanism

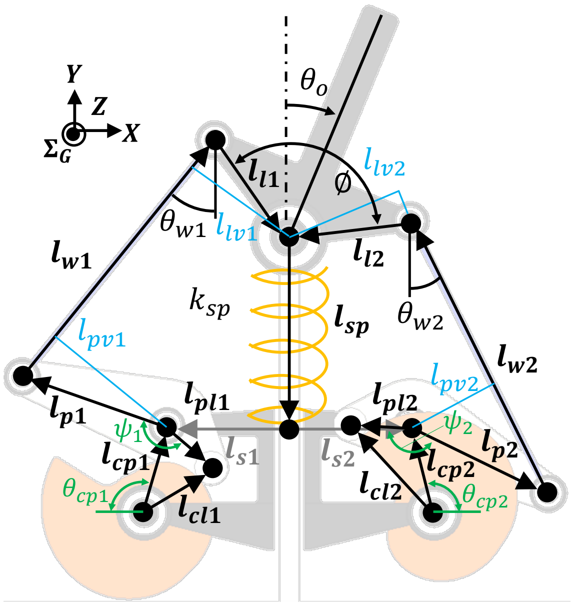

Fig.2 Link vectors in the proposed mechanism

Then, the translational movement of the slider is converted to the rotational movement of the output link via the wire. Thus, swift rotary motion is realized. For stiffness control, the magnitude of stiffness of the main joint can be changed. In a fully compressed spring, as shown in Fig. 1 (c), the two wires will experience more tension than if the spring were not compressed. When the two cams are maintained in this state and a force is applied to the output link from the outside, the reaction force of the output link becomes larger than that in the state in which the spring is not compressed. Owing to these characteristics, the mechanism can change the amount of compression of the spring and the rigidity of the main joint by controlling the postures of the two cams.

We derived a mathematical model for rapid motion. First, consider the torque generated in the output link from a static point of view. Fig. 2 shows the link vector of the proposed mechanism, and Table 1 lists the variables considered in the analysis. The force $\boldsymbol{F_{sp}}$ applied to the slider is determined by $\boldsymbol{\delta_{sp}}$ and k_{sp}:

$$\boldsymbol{\delta_{sp}} = \boldsymbol{L_{spn}} - \boldsymbol{l_{sp}} \tag{1}$$

$$\boldsymbol{F_{sp}} = k_{sp}\boldsymbol{\delta_{sp}} \tag{2}$$

where δ_{sp} is the spring displacement vector; L_{spn}; l_{sp} is the slider position vector; and k_{sp} is the spring constant. L_{spn} represents the natural length of the spring.

Table 1 Variables used for analyzing the joint mechanism

$\boldsymbol{l_x}$	Link vector ($x = l*,w*,p*,cp*,cl*,pl*,s*,sp$)
l_{lv*}	Scalar projection of $\boldsymbol{l_{l*}}$
l_{pv*}	Scalar projection of $\boldsymbol{l_{p*}}$
θ_o	Absolute angle of output link
$\emptyset$	Angle between $\boldsymbol{l_{l1}}$ and $\boldsymbol{l_{l2}}$
θ_{w*}	Absolute angle of wire
k_{sp}	Spring constant
$\boldsymbol{F_{sp}}$	Force vector of spring
$\boldsymbol{F_{w*}}$	Tension vector of wire
T_o	Torque of output link
T_{c*}	Torque of motor
T_{p*}	Torque of passive link
$\boldsymbol{v_l}$	Velocity vector of slider
$\dot{\theta}_o$	Angular velocity of output link
ψ_*	Angle between $\boldsymbol{l_{p*}}$ and $\boldsymbol{l_{pl*}}$
θ_{cp*}	Absolute angle of $\boldsymbol{l_{cp*}}$
$*$	Index 1 or 2

The thrust $\boldsymbol{F_{sp}}$ of the slider is transmitted to the output link via the wire. The force F_{w*} generated on the wire is expressed as shown in the following equation.

$$F_{w*} = \frac{|\boldsymbol{F_{sp}}|}{cos\theta_{w*}} \tag{3}$$

where θ_{w*} is the angle of the wire.

By using the Jacobian matrix $\boldsymbol{J_{sp*}} = (\boldsymbol{l_{l*}} \times \boldsymbol{e_z})$ derived from the outer product of the force $\boldsymbol{F_{w*}}$ generated on the wire and the rotation direction vector $\boldsymbol{e_z}$, the torque T_o generated in the output link is obtained.

$$T_o = \boldsymbol{J_{sp*}^T}\boldsymbol{F_{w*}} \tag{4}$$

Further, the reduction ratio, which represents the relationship between the input and output when the force $\boldsymbol{F_{sp}}$ generated by the spring is converted into the torque T_o of the output link, is expressed as follows.

$$G_{sp} = \frac{T_o}{|\boldsymbol{F_{sp}}|} \tag{5}$$

During rapid motion, the slider, two wires, and an output link are the elements that move. Among these elements, the inertial force of the slider and the output link is large and cannot be ignored. We calculated the velocity from the viewpoint of energy loss. The energy balance during the rapid motion is expressed as follows:

$$\frac{1}{2}m_l v_l^2 + \frac{1}{2}I_o\dot{\theta}_o^2 = E - \frac{1}{2}k_{sp}|\boldsymbol{\delta_{sp}}|^2 \tag{6}$$

where the mass of the slider is m_l; velocity, v_l; inertia of the output link, I_o; angular velocity, $\dot{\theta}_o$; and energy completely accumulated in the spring, E

Further, v_l can be expressed using G_{sp} from equations (5), and $\dot{\theta}_o$ as follows.

$$v_l = G_{sp}\dot{\theta}_o \tag{7}$$

From equations (6) and (7), the angular velocity $\dot{\theta}_o$ of the output link can be expressed as follows.

$$\dot{\theta}_o = \sqrt{\frac{2E - k_{sp}|\boldsymbol{\delta_{sp}}|^2}{m_l G_{sp}^2 + I_o}} \tag{8}$$

3. Design of the cam mechanism

The design method of the cam mechanism that can compress the spring while maintaining the posture of the output link and the operating points related to the motor torque and angular velocity as constant as possible is described in this section. When designing the cam mechanism using this method, the designer should proceed in the following order.

1. Basic machine parameters, such as motor and link ratio
2. Design of the spring constant of the linear motion spring used
3. Cam design

For basic machine parameters, the link ratio of link unit, instantaneous angular velocity $\dot{\theta}_{pf*}$ of the passive link in the fully compressed state of spring, motor torque T_{c*} during spring compression, and motor angular velocity $\dot{\theta}_{c*}$ must be selected. For deciding the link ratio, it is necessary to determine l_{l*}, ϕ , l_w, l_p l_b, l_{spn}, and l_{spf} based on the output characteristics required for the application. Further, $\dot{\theta}_{pf*}$ needs to be determined from the time that can be spent compressing the spring. T_{c*} and $\dot{\theta}_{c*}$ during spring compression are steady values. For example, it is necessary to select an operating point or limit operating point that is efficient for the actuator. These parameters are also the parameters that are to be changed if the designed cam does not meet the constraints such as the size of the mechanism. The Further, $\dot{\theta}_{pf*}$ needs to be adjusted if the motor does not satisfy the constraints.

After determining the four abovementioned parameters, the spring constant and the cam should be designed.

3.1. Design of the spring constant

In designing the cam, the characteristic of the reduction ratio curve required for the cam is greatly affected by the magnitude of the spring constant. We determined the spring constant by modeling the fully compressed spring using the four abovementioned parameters.

In the fully compressed state of spring, torque T_{pf*} generated in the passive link can be expressed using motor torque T_{c*}, angular velocity $\dot{\theta}_{c*}$, and angular velocity of passive link $\dot{\theta}_{pf*}$ as follows.

$$T_{pf*} = \frac{T_{c*}\dot{\theta}_{c*}}{\dot{\theta}_{pf*}} \tag{9}$$

The tension F_{wf*} generated on the wire on the release side is expressed as follows.

$$F_{wf*} = \frac{T_{pf*}}{l_{pv*}} \tag{10}$$

When the spring is fully compressed, the output link has to maintain the posture immediately before starting the rapid motion. To achieve this, the resultant force of the output torque, which is exerted by the tension of the left and right wires, must be 0. That is, to maintain the antagonistic state, the following formula should be satisfied:

$$F_{wf1}l_{lv1} - F_{wf2}l_{lv2} = 0 \tag{11}$$

From equation (11), F_{wf1} and F_{wf2} are related as follows.

$$F_{wf2} = \frac{l_{lv1}}{l_{lv2}}F_{wf1} \tag{12}$$

Thus, it is seen that the magnitudes of the forces generated on the two wires are different. From the relationship between the force applied to the spring and the amount of displacement of the spring, the spring constant k_{sp} can be calculated as follows using equation (13).

$$k_{sp} = \frac{F_{wf1} \cos \theta_{w1} + F_{wf2} \cos \theta_{w2}}{|\boldsymbol{\delta}_{sp}|} \tag{13}$$

From equations (9), (10), and (13), it can be seen that k_{sp} greatly contributes to the torque T_{c*} and angular velocity $\dot{\theta_{c*}}$ of the motor, the link ratio, and the angular velocity $\dot{\theta_{pf*}}$ of the passive link.

3.2. Design of the cam

In the proposed mechanism, the cam has two types of movement areas and one stop area. Fig. 3 shows the configuration for cam allocation. The movement areas are used to move the release side passive link and contraction side passive link. The stop area is for receiving followers after the release operation. In designing the cam curve, first the torque generated in the passive link during the spring compression process should be considered. The torque T_{p*} generated in the passive link can be expressed from the tension F_{w*} generated in the wire during the spring contraction process as follows.

$$T_{p*} = F_{w*} l_{pv*} \tag{14}$$

Here, F_{w*} can be expressed by using the following formula using the relation between equations (12) and (13).

$$F_{w*} = \frac{l_{lv*} k_{sp} |\boldsymbol{\delta}_{sp}|}{l_{lv2} \cos \theta_{w1} + l_{lv1} \cos \theta_{w2}} \tag{15}$$

For the motor and cam to generate the torque T_{p*} in the passive link, the cam should have a reduction ratio G_{c*} as follows.

$$G_{c*} = \frac{T_{p*}}{T_{c*}} \tag{16}$$

Equation (16) does not take into consideration the torque required to accelerate each machine element, Coulomb friction, viscous friction, etc. At the time of initial movement, the force stored in the spring is very small, and hence, the reduction ratio G_{c*} of the cam becomes extremely small, and the angular velocity of the passive link diverges. Hence, the following equation is applied in the design to prevent this phenomenon.

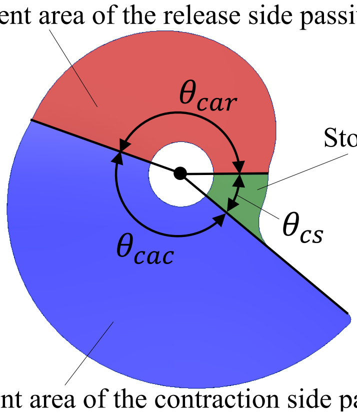

Fig.3 Configuration for cam allocation

$$\theta_{pi*} = \sum_{\theta_{c*}=\Delta\theta_{ca\star}}^{\lambda_\star} \frac{\lambda_\star}{\theta_{c*}} G_{c*}(\theta_{c*}) \Delta\theta_{ca\star} \tag{17}$$

Here, θ_{pi*} indicates the movement amount of the passive link at the time of initial movement, and $\Delta\theta_{ca\star}$ indicates the minute rotation amount of the cam. Further, $\lambda_\star$ is a constant for adjusting the reduction ratio. The total movement of the moment arm during the compression process of the spring θ_{pf*} is expressed using θ_{pi*} and cam allocation angle $\theta_{ca\star}$ as follows:

$$\theta_{pf*} = \sum_{\theta_{c*}=\lambda_\star}^{\theta_{ca\star}} G_{c*}(\theta_{c*}) \Delta\theta_{ca\star} + \theta_{pi*} \tag{18}$$

The designer needs to optimize the parameters $\lambda_\star$ and $\dot{\theta_{pf\star}}$ to equalize the movement amount of the required specifications with θ_{pf*} calculated using equation (18). The displacement of θ_{p*} with respect to the displacement amount of θ_{c*} can be expressed as follows:

$$\theta_{p*} = \sum_{\theta_{c*}=\Delta\theta_{ca\star}}^{n} \frac{\lambda_\star}{\theta_{c*}} G_{c*}(\theta_{c*}) \Delta\theta_{ca\star} \quad (\Delta\theta_{ca\star} \le n \le \lambda_\star) \tag{19}$$

$$\theta_{p*} = \sum_{\theta_{c*}=\Delta\theta_{ca\star}}^{n} G_{c*}(\theta_{c*}) \Delta\theta_{ca\star} + \theta_{pi*} \quad (\lambda_\star < n \le \theta_{ca\star}) \tag{20}$$

By substituting an arbitrary θ_{c*} for the variable n in equations (19) and (20), an arbitrary θ_{p*} can be known. From equations (19) and (20), l_{cl*} becomes clear from the geometrical relation. As shown in Fig. 4, the vector

${}^{c}\boldsymbol{l}_{cl*}$ for determining the coordinate point of the cam curve can be calculated by the following formula in terms of the rotation matrix $\boldsymbol{R}(-\theta_{c*})$:

$$ {}^{c}\boldsymbol{l}_{cl*} = \boldsymbol{R}(-\theta_{c*})\boldsymbol{l}_{cl*} \tag{21} $$

Fig. 5 shows the contour curve of the cam created by calculating the coordinate points of the cam curve from equation (21) and using 3DCAD. The contour curve of the cam is obtained using the corresponding parameters listed in Table 2.The contour curve is drawn by complementing the coordinate points with the spline curve and is offset outward by the size of the radius of the follower. Fig. 6 shows the movement of the passive link with respect to the movement of the cam. When θ_c is displaced from 0° to 160°, the slope of the curve becomes gentle. This means that the reduction ratio is increased with respect to the increase in the compression amount of the spring to counter the gradually increasing reaction force of the spring.

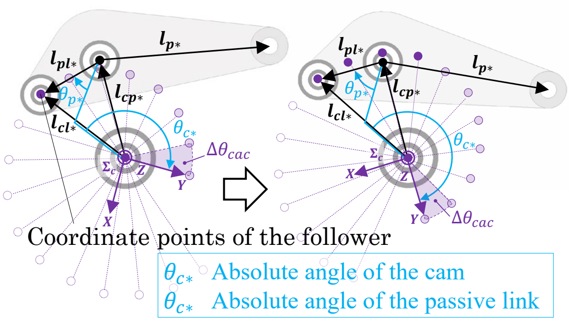

Fig.4 Design of the pitch curve

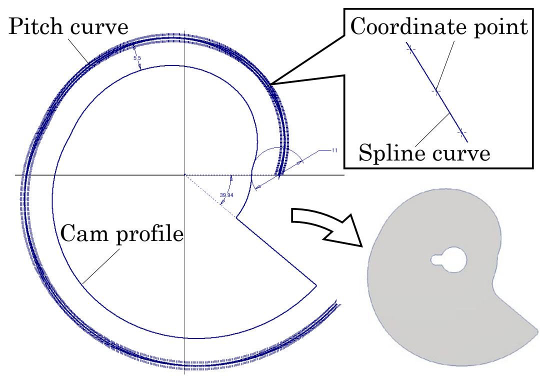

Fig.5 Designed cam shape

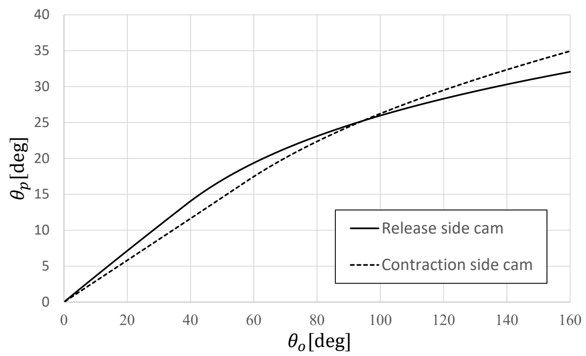

Fig.6 Theoretical cam curves

Table 2. Specifications of the device

l_{l*}	Length of $\boldsymbol{l}_{l*}$	0.0599[m]
l_{w*}	Length of $\boldsymbol{l}_{w*}$	0.215[m]
l_{p*}	Length of $\boldsymbol{l}_{p*}$	0.08[m]
l_{pl*}	Length of $\boldsymbol{l}_{pl*}$	0.02[m]
l_{s*}	Length of $\boldsymbol{l}_{s*}$	0.0285[m]
l_{spn}	Length of $\boldsymbol{l}_{spn}$	0.211[m]
δ_{sp}	Length of $\boldsymbol{\delta}_{sp}$	0.0460[m]
$\emptyset$	Direction of $\boldsymbol{l}_{l*}$	115°
ψ_*	Angle between $\boldsymbol{l}_{p*}$ and $\boldsymbol{l}_{pl*}$	155°
θ_{cp*}	Absolute angle of $\boldsymbol{l}_{cp*}$	105°
λ_c	Constant for adjusting of the contraction side	38.9°
λ_r	Constant for adjusting of the release side	57.4°
θ_{cac}	Contraction side cam allocation angle	160°
θ_{car}	Release side cam allocation angle	160°
θ_{cs}	Stop area angle	40°
$\Delta\theta_{ca*}$	Minute rotation amount of cam	0.350°
θ_{max}	Maximum movement range	+22.5°
θ_{min}	Minimum movement range	-22.5°
k_{sp}	Spring constant	3810[N/m]
m_l	Mass of Slider	1.03[kg]
I_o	Inertia of Output link	0.00598[kgm^2]
T_{c*}	Motor torque	0.65[Nm]
$\dot{\theta}_{c*}$	Motor angular velocity	2.72[rad/s]
$\dot{\theta}_{pfc}$	Contraction side angular velocity of passive link in the fully compressed state of spring	0.224[rad/s]
$\dot{\theta}_{pfr}$	Release side angular velocity of passive link in the fully compressed state of spring	0.338[rad/s]

4. Performance evaluation test

To compare the theoretical value and the measured value for torque and angular velocity during rapid motion, we evaluated the performance using an experimental device. The appearance of the device is shown in Fig. 7, and the design parameters are listed in Table 2. Silicon oil is applied to the linear shaft to improve the sliding performance of the actual machine. Fig. 8 shows the angle of the output link with respect to the measured elapsed time in the real machine. This actual measurement value was calculated based on the pixel value of the captured image depicting the motion of the output link.

Fig. 9 shows the results of comparing the theoretical and measured values for the angular velocity of the output link. The theoretical value was calculated using equation (8). The measured value was calculated by generating a three-dimensional approximation curve based on the angle data in Fig. 8 and by numerically differentiating the approximation curve. As a result, although the two waveforms show the same tendency, it can be confirmed that the experimental value is slightly below the theoretical value and the error gradually increases. This factor is considered to be the loss due to Coulomb friction and viscous friction generated between the slider and the shaft, which is not theoretically modeled. Furthermore, one of the factors could be that the compression amount of the spring does not reach the design value due to the elastic deformation of the wires and links. Further, since the speed increases in the latter half of the operation, the influence of viscous friction proportional to the square of the speed is considered to be dominant.

Fig. 10 shows a comparison of the theoretical and the actual measured values of the output link torque. The theoretical value was calculated using equation (4). The measured value was obtained by numerically differentiating the approximate curve in Fig. 8 to calculate the angular acceleration and was calculated using equation (22).

$$T_o = I_o \ddot{\theta}_o \tag{22}$$

As seen from Fig. 10, the error is larger than the angular velocity because the mass of the slider and the loss due to viscous friction is not considered in equation (4).

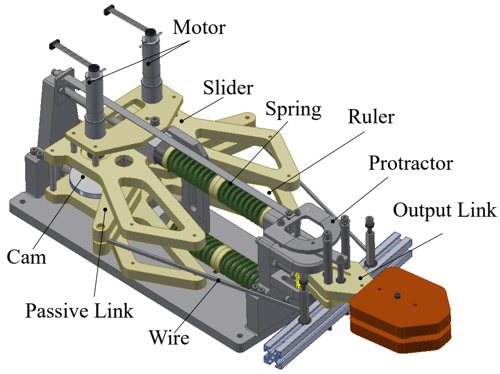

Fig.7 Experimental device

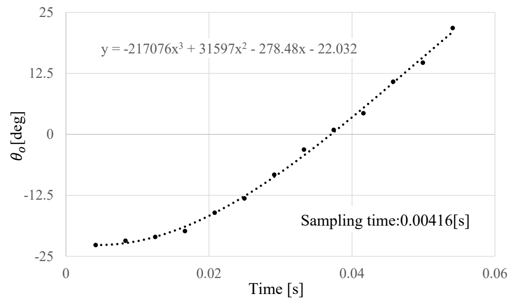

Fig.8 Measurement angle and approximate curve

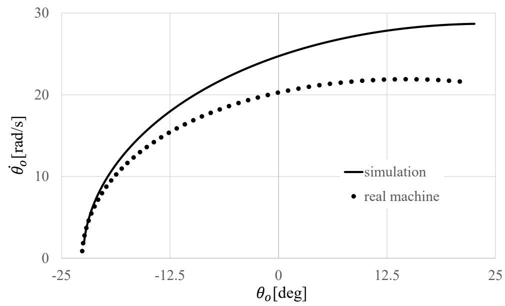

Fig.9 Angular velocity of the output link

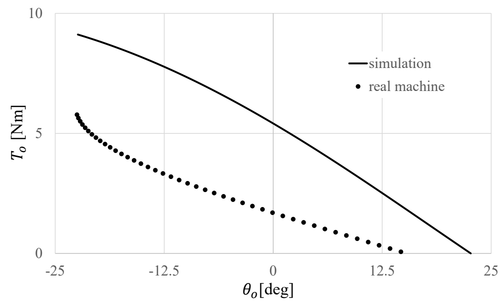

Fig.10 Torque of the output link

5. Conclusion

In this paper, we propose a special mechanism with three functions: normal motion, rapid motion, and rigidity control of the main joint. The motion principle of the mechanism and the design principle of the cam are discussed in this paper. Finally, we built a real machine and discussed the effectiveness of the proposed mechanism. It was shown that in the cam design principle, by dividing the cam area appropriately, different reduction ratio curves can be set arbitrarily on the contraction and release sides. By using the design principle, the posture of the output link can be maintained, and the spring can be compressed efficiently. In the performance evaluation of the rapid motion of the real machine, we found that the measured value was lower than the theoretical value because of the effect of viscous friction between the shaft and slider. However, the error was small, and the validity of the mathematical model was confirmed. As future research subjects, we will evaluate the effectiveness of normal motion and rigidity control of the main joint by using an actual machine.

References

1. M.H.Raibert, H.B.Brown, Jr., Chepponis, "Experiments in balance with a 3D one-legged hopping machine," Int. J. Robot. Res., vol.3, no.2,pp.75-92, 1984
2. M. Raibert, "Legged Robots that balance," MIT Press, Cambridge, 1986
3. H. Okubo, M. Handa, E. Nakano, "Design of a Jumping Machine Using Self-energizing Spring-Jumping by Small Actuators," Journal of Robotics Society of Japan, vol.16, no.5, pp.57-63, 1988
4. S. Hyon and T. Mita, "Development of a biologically inspired hopping robot-Kenken," Proc. of IEEE International Conference on Robotics and Automation, pp. 3984-3991, 2002
5. K. Arikawa and T. Mita, "Design of Multi-DOF jumping robot," Proc. of IEEE International Conference on Robotics and Automation, pp. 3992-3997, 2002
6. S. Hyon, N. Yokoyama, T. Emura, "Back Handspring of a Multi-link Gymnastic Robot- Reference model approach," Advance Robotics, vol. 20, no.1, pp. 93-113, 2006
7. A.A. Nassiraei,K. et. al., Realization of Rapid Movement for Legged Entertainment Robots Using Two New Actuators, the Inertia Actuator and the Cam Charger,Journal of Advanced Computational Intelligence, Vol.11 No.8, pp.979 - 988, 2007
8. A.A. Nassiraei,K. et. al., Development of an Artistic Robot "Jumping Joe", Proc. of IEEE IROS'06, pp.1720 - 1725, 2006
9. NAKAMURA, Taro; SHINOHARA, Hitomi. Position and force control based on mathematical models of pneumatic artificial muscles reinforced by straight glass fibers. In: Proceedings 2007 IEEE International Conference on Robotics and Automation. IEEE, 2007. p. 4361-4366.
10. T. Tanaka and S. Hirose, "Development of Leg-Wheel Hybrid Quadruped "AirHopper": Lightweight Leg-Wheel Design," J. of Robotics and Mechatronics, Vol.20, No.4, pp. 533–540, 2008.
11. YAMADA, Atsushi, et al. A compact jumping robot utilizing snap-through buckling with bend and twist. In: 2010 IEEE/RSJ International Conference on Intelligent Robots and Systems. IEEE, 2010. p. 389-394.
12. Sonoda, Takashi, et al. "Development of antagonistic wire-driven joint employing kinematic transmission mechanism." Journal of Automation Mobile Robotics and Intelligent Systems 4 (2010): 62–70.
13. Nishida, Yuya, Takashi Sonoda, and Kazuo Ishii. "Jacobian Matrix Derived from Cross Product and its Application into High Power Joint Mechanism Analysis." Journal of Bionic Engineering 7 (2010): S218–S223.
14. Yuya Nishida, et. al., "Design Principle of High Power Joint Mechanism Possible to Walking and Jumping Imitating Locust Leg Structure," Journal of Robotics and Mechatronics, Vol.23, No.2, pp.225–230, 2011
15. H. C. Bannet-Clark, "The energetic of the Locust Schistocerca gregaria," J. of Experimental Biology, Vol.63, pp. 53–83, 1975.
16. W. J. Heitler, "The Locust Jump," J. of Comparative Physiology A: Neuroethology, Sensory, Neural, and behavioral physiology, Vol.89, No.1, pp. 93–104, 1974.
17. A.A.F Nassiraei, et al., Realization of the Rapid Movements for the Entainment Robots by Using Two New Actuators"Inertia Actuator" &"Cam Charger," Proc. ASME IMECE2006, IMECE2006–14257, 2006
18. M. Kovac, M. Fuchs, and A. Guignard, "Jean-Christophe Zufferey, Dario Floreano, A mimiature 7g jumping robot," Proc. of the IEEE Int. Conf. on Robotics and Automation (ICRA'2008), pp. 373–378,2008.

AROB Jimukyoku
Journal of Advances in Artificial Life Robotics, Vol. 1, No. 3 (December 2020) 143-151

Authors Introduction

Mr. Katsuaki Suzuki

He received his Master's degree from the Department of Human Intelligence Systems, Graduate School of Life Science and Systems Engineering, Kyushu Institute of Technology, Japan in 2017. He is currently a doctoral student in Kyushu Institute of Technology, Japan.

Dr. Yuya Nishida

He is an Associate Professor at Graduate School of Life Science and System Engineering, Kyushu Institute of Technology, Japan. His research interests include filed robotics, its application, and data processing.

Dr. Takashi Sonoda

He is an Associate Professor at Department Integrated System Engineering, Nishi-Nippon Institute of Technology, Fukuoka, Japan. His research interests are underwater robotics and robot manipulator systems.

Prof. Kazuo Ishii

He is a Professor at Graduate School of Life Science and System Engineering, Kyushu Institute of Technology, Japan. His research intetrests include field robots and intelligent robot systems.